

A 52 hours VLT/FORS2 spectrum of a bright $z \sim 7$ HUDF galaxy: no $Ly\alpha$ emission. \star

E. Vanzella¹, A. Fontana², L. Pentericci², M. Castellano², A. Grazian², M. Giavalisco⁴, M. Nonino³, S. Cristiani³, G. Zamorani¹, and C. Vignali⁵

¹ INAF - Osservatorio Astronomico di Bologna, via Ranzani 1, I-40127 Bologna, Italy

² INAF - Osservatorio Astronomico di Roma, via Frascati 33, 00040, Monteporzio, Italy

³ INAF - Osservatorio Astronomico di Trieste, via G. B. Tiepolo 11, I-34131, Trieste, Italy

⁴ Department of Astronomy, University of Massachusetts, 710 North Pleasant Street, Amherst, MA 01003, USA

⁵ Dipartimento di Fisica e Astronomia, Universita' degli Studi di Bologna, Viale Berti-Pichat 6/2, 40127 Bologna, Italy

Received -; accepted -

ABSTRACT

Aims. We aim to determine the redshift of *GDS_1408*, the most solid $z \sim 7$ galaxy candidate lying in the Hubble Ultra Deep Field.

Methods. We have used all the VLT spectra of *GDS_1408* collected by us and two other groups with FORS2 at VLT in the last five years, for a total integration time of 52hr. The combined spectrum is the deepest ever obtained of a galaxy in the Reionization epoch.

Results. We do not detect any emission line or continuum over the whole wavelength range, up to 10100Å. Based on an accurate set of simulations, we are able to put a stringent upper limit of $f(Ly\alpha) < 3 \times 10^{-18} \text{ erg/s/cm}^2$ at 3-9 sigma in the explored wavelength range, corresponding to a rest-frame equivalent width $EW < 9 \text{ \AA}$. Combining this limit with the SED modelling we refine the redshift to be $z = 6.82 \pm 0.1$ (1-sigma). The same SED fitting indicates that *GDS_1408* is relatively extinct ($A_{1600} \approx 1$) with a dust corrected star formation rate of $\approx 20 M_{\odot} \text{ yr}^{-1}$. The comparison between the un-attenuated equivalent width predicted by the case-B recombination theory and the observed upper limit, provides a limit on the effective $Ly\alpha$ escape fraction of $f_{esc}^{eff}(Ly\alpha) < 8\%$. Even though we cannot rule out a major contribution of the inter/circum galactic medium in damping the line, a plausible interpretation is that *G2_1408* is moderately evolved and contains sufficient gas and dust to attenuate the $Ly\alpha$ emission, before it reaches the intergalactic medium.

Conclusions. The redshift confirmation of even the best $z \approx 7$ candidates is very hard to achieve (unless the $Ly\alpha$ or unusually strong rest-UV nebular emission lines are present) with the current generation of 8-10m class telescopes. We show that both JWST and E-ELT will be necessary to make decisive progresses. Currently, the increased redshift accuracy obtained with this kind of analysis makes ALMA an interesting option for the redshift confirmation.

Key words. Galaxies: high - redshift; Galaxies: formation; Galaxies: distances and redshifts

1. Introduction

Understanding the process of reionization of the intergalactic medium in the early Universe and the nature of the first galaxies responsible for that process are among the most important goals of modern cosmology (Robertson et al. 2010, and references therein). Thanks to the deep and panchromatic data, such as GOODS, CANDELS and Hubble Ultra Deep Field (HUDF), great progress has been made in our ability to identify and subsequently confirm (spectroscopically) galaxies at $z < 7$. The most prominent spectral feature in the UV rest-frame wavelengths probed by optical/NIR spectroscopy at $z \approx 7$ is the $Ly\alpha$ emission line (e.g., Vanzella et al. 2011, V11; Pentericci et al. 2011; Pentericci et al. 2014, P11, P14; Schenker et al. 2012; Schenker et al. 2014, Ono et al. 2012, Shibuya et al. 2012). However, at $z > 7$ the situation is still challenging and at present only a handful objects are spectroscopically secured. There are at least two main reasons: (1) Physical processes in the galaxies: the $Ly\alpha$ emission is a resonant atomic transition very sensitive to dust attenuation, and can be used for a diagnostic of the physical processes occurring within the galaxy (Giavalisco et al.

1996; Atek et al. 2013), since its strength and velocity profile depend on the instantaneous star formation rate, gas and dust content, metallicity, kinematics, and geometry of the interstellar medium. Therefore an evolution of the average galaxy properties with time (gas and/or dust properties and/or ionizing emission) can make it intrinsically absent at specific cosmic epochs. (2) Reionization: the $Ly\alpha$ emission line may suffer of damping effect due to an increase of the neutral gas fraction in the intergalactic and/or circum galactic media (Miralda-Escudé et al. 2000; Dijkstra et al. 2011; Treu et al. 2012) or a increasing incidence of optically thick absorption systems (Bolton & Haehnelt 2013) as the ending phase of the reionization is approached. Another limiting effect was instrumental: efficient near infrared spectrographs ($\lambda \gtrsim 1\mu\text{m}$) with multiplexing capabilities are needed to capture UV rest-frame features for many targets at once, and only recently they are becoming available (e.g., VLT/KMOS, Keck/MOSFIRE, LBT/LUCI).

While point (1) is alleviated by the fact that (on average) the frequency of $Ly\alpha$ line emitters appear to increase as redshift increases ($3 < z < 6.5$, Ouchi et al. 2008; Schaerer et al. 2011; Stark et al. 2011), the damping due to reionization may severely limit our current ability to confirm galaxies at $7 < z < 10$ (but see Dijkstra & Wyithe 2010). Finkelstein et al. (2013) find only one galaxy at $z = 7.51$ out of 43 candidates at $z > 6.5$ with

\star This work is based on data collected at ESO VLT (prog.ID 084.A-0951(A), 086.A-0968(A), 088.A-1013(A) and 088.A-1008(A)), and at NASA HST.

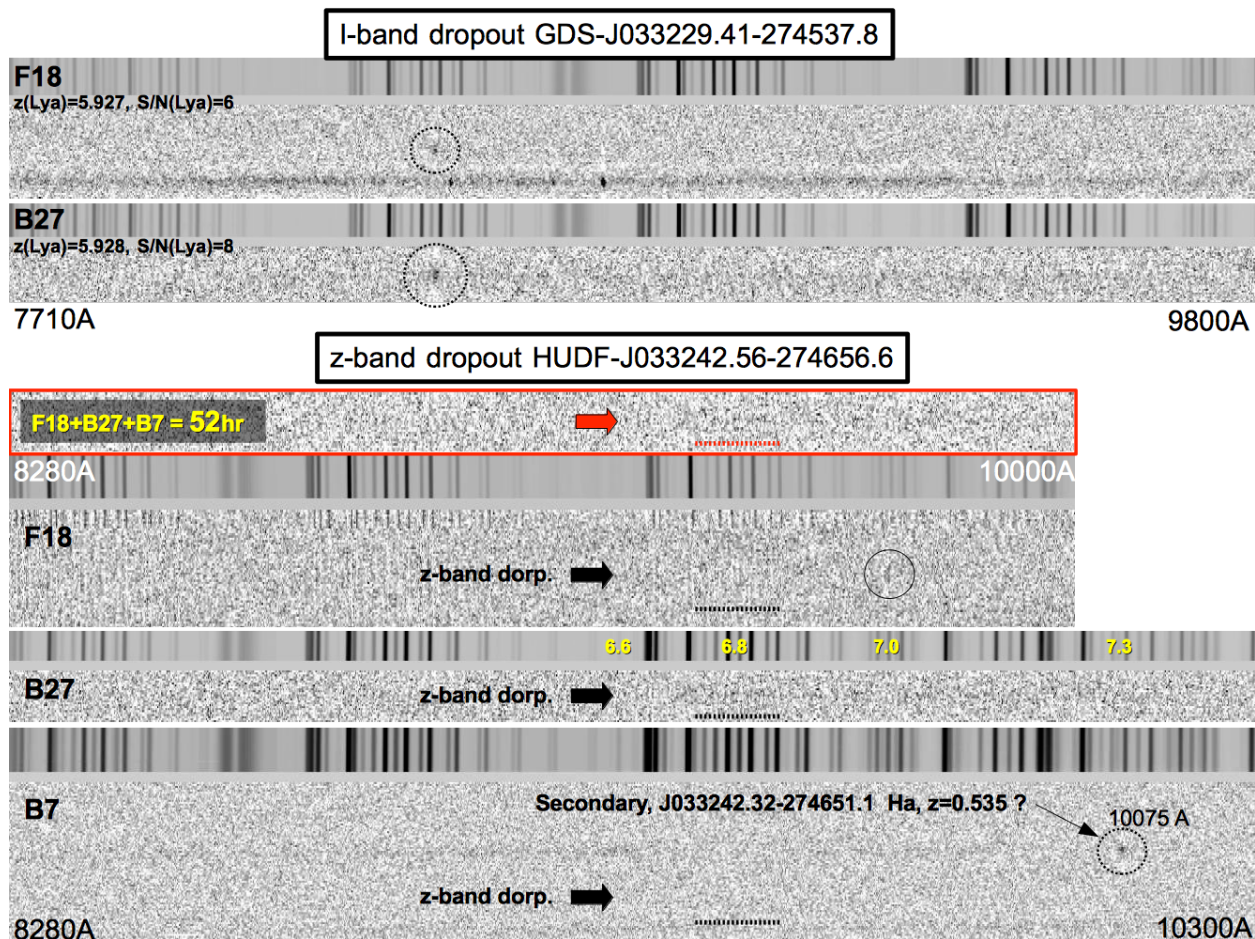


Fig. 1. Two dimensional signal to noise spectra and sky spectra of the galaxies discussed in the text. **Top:** spectra of the i-band dropout GDS J033229.41-274537.8 observed in F18 (upper part) and B27 (lower part). The $L\gamma\alpha$ line is marked with a dotted circle. **Bottom:** the stacked 52hr spectrum of the z-band dropout $G2_1408$ is shown, with the individual spectra of F18, B27, B7 (lower part). The expected position of the $L\gamma\alpha$ continuum break is marked with dotted horizontal lines (see text). In the B27 spectrum the redshift values are reported above the sky as a reference. In the F18 spectrum the dotted circle marks the older (here revisited) feature discussed in Fontana et al. (2010). B7 spectrum shows also the $H\alpha$ emission from the secondary object J033242.32-274651.1 at $z=0.535$, useful here as an example of a still performing FORS+600z configuration beyond one micron.

the Keck/MOSFIRE and similarly Schenker et al. (2014) find only one possible $L\gamma\alpha$ line at $z = 7.62$ in their sample of 19 $z \sim 8$, remarking that some process is making the $L\gamma\alpha$ difficult to detect. Therefore, there is a large fraction of non- $L\gamma\alpha$ emitters lying well within the first Gyr after the Big-Bang, whose nature is worth to investigate. Clearly, all these explanations assume that the efficiency of the color selection based on the $L\gamma\alpha$ -break remains extremely high at $z \geq 7$, i.e. that most of current $z \geq 7$ candidates are indeed at their estimated redshifts.

In this work, we report on an ultradeep spectrum (52 hours integration) of the brightest $z \simeq 7$ galaxy in the Hubble Ultra Deep Field ($F125W = 26.1 \pm 0.02$). Being by far the brightest $z \simeq 7$ candidate in this well-studied region, it has been continuously selected as a high redshift candidate from the earliest NICMOS to the current ultradeep HUDF data, at variance with other targets (Yan & Windhorst 2004; Bouwens et al. 2004; Bouwens & Illingworth 2006; Labbé et al. 2006; Bouwens et al. 2008; Oesch et al. 2010; Fontana et al. 2010; McLure et al. 2010; Bunker et al. 2010; Yan et al. 2010; Finkelstein et al. 2010; Castellano et al. 2010; Wilkins et al. 2011; Bouwens et al. 2011; Grazian et al. 2011; McLure et al. 2013; Bouwens et al. 2014). We focus here on the combination of ultradeep spectroscopy and photometry to derive new insights about its nature.

Errors are quoted at the 1σ confidence level, unless otherwise stated. Magnitudes are given in the AB system ($AB \equiv 31.4 - 2.5 \log(f_\nu/nJy)$). We assume a cosmology with $\Omega_{tot}, \Omega_M, \Omega_\Lambda = 1.0, 0.3, 0.7$ and $H_0 = 70 \text{ km s}^{-1} \text{ Mpc}^{-1}$.

2. FORS2 Observations and Data Reduction

HUDF-J033242.56-274656.6 galaxy ($G2_1408$ in Castellano et al. 2010 and hereafter) has been observed through four different VLT/FORS programs collected in the period 2009-2012, 084.A-0951(A) (P.I. A. Fontana), 086.A-0968(A)–088.A-1013(A) (P.I. A. Bunker), 088.A-1008(A) (P.I., R. Bouwens), and 283.A-5063 (P.I., M. Carollo) with exposure times of 18 (Fontana, F18), 27 (Bunker, B27), 7 (Bouwens, B7) and 8 (Carollo, C8) hours on target, respectively, for a total of $\simeq 60$ hours integration time. Unfortunately, in the program 283.A-5063 the $G2_1408$ source was placed at a position where the CCD has a defect and no dithering has been performed, therefore we exclude the 283.A-5063 program from the following analysis. The total usable exposure time is 52 hours. The median seeing was ~ 0.8 arcsecond in all runs. The F18 data were presented in Fontana et al. (2010) where we reported a tentative detection of a $L\gamma\alpha$ line at $z=6.972$. The other runs, B27 and B7, have been obtained subsequently in many dif-

ferent nights (especially B27), and particular care has been devoted to the alignments of the frames by using bright sources and sky emission lines. The B27 program has also been presented in Caruana et al. (2013), where they reported a $S/N \simeq 3.2$ at the location of the putative $Ly\alpha$ at $z = 6.972$. We discuss in very detail any possible presence of $Ly\alpha$ emission by combining all the available programs.

Data reduction has been performed as in Vanzella et al. (2011), with particular care to the sky subtraction. The classical ‘‘A-B’’ dithering scheme that combines the partial frames (A-B) and (B-A) is performed, with an additional treatment that *equalizes* for local differences in the number counts between frames (e.g., due to time variation of sky lines, distortion, etc.). The algorithm implements an ‘‘A-B’’ sky subtraction joined with a zero (e.g., median) or first order fit of the sky along columns that regularized possible local differences in the sky counts among the partial frames before they are combined. Finally, the two-dimensional spectra have been combined with a weighted average, and the subsequent resulting spectrum has been flux and wavelength calibrated. The two dimensional sky-subtracted partial frames are also combined (in the pixel domain) to produce the weighted RMS map, associated to the final reduced spectrum. This allows us to calculate the two dimensional signal to noise spectra, useful to access the reliability of the spectral features (as we address below with simulations).

Further checks have been performed on other targets placed in the masks and on those in common between F18 and B27. In particular, Caruana et al. (2013) targeted the same faint i -band dropout we confirmed previously with F18 (Fontana et al. 2010), GDS J033229.41-274537.8 at $z = 5.927$. While in the F18 spectrum the continuum is not detected, in our B27 spectrum we find a very faint trace redward of the line and a $Ly\alpha$ with estimated flux of 3.8×10^{-18} erg/s/cm² at $S/N \simeq 8$, about a factor 1.25 higher than F18, whose flux is estimated to be $\simeq 3.0 \times 10^{-18}$ erg/s/cm² with $S/N \simeq 6.5$. Both flux and error estimates are compatible within the flux calibration accuracy and different integration time. The top part of Figure 1 shows the S/N spectra of the $z = 5.927$ galaxy (i.e., the reduced spectrum divided by its RMS map).

Following the above approach, we have combined the 52 hours of observations of *GDS_1408*. The three individual S/N spectra and the combined one are shown in the bottom part of Figure 1. The 52 hours spectrum is the deepest spectroscopic observation of a $z \sim 7$ galaxy obtained to date.

3. Results

Before discussing any feature in the spectrum we note that the available photometry already constrains the redshift in the range ($6.5 < z < 7.0$) where FORS2 is an efficient instrument for the detection of the corresponding $Ly\alpha$, both in terms of wavelength coverage and response. First, we recall that globally the high redshift nature ($z > 6.5$) is guaranteed by the large observed break between the ultradeep optical and near infrared bands ($\Delta m \simeq 4$ magnitudes) and the well determined flat behaviour of the SED in the near infrared bands, detected with a high SNR (HST-WFC3, $S/N \simeq 20-50$), as shown in Figure 2 and 3. This makes *GDS_1408* one of the most robust $z \sim 7$ candidates. Second, a reliable upper limit on the redshift is provided by the clear detections in the z_{850} band ($z < 7.3$) and narrow band filter, NB973 ($z < 7$), centered at $\lambda = 9755\text{\AA}$ and $d\lambda = 200\text{\AA}$ (Figure 3). The limit provided with the 3σ detection in the NB973 is $z < 6.94$ if the entire NB973 filter is capturing the galaxy con-

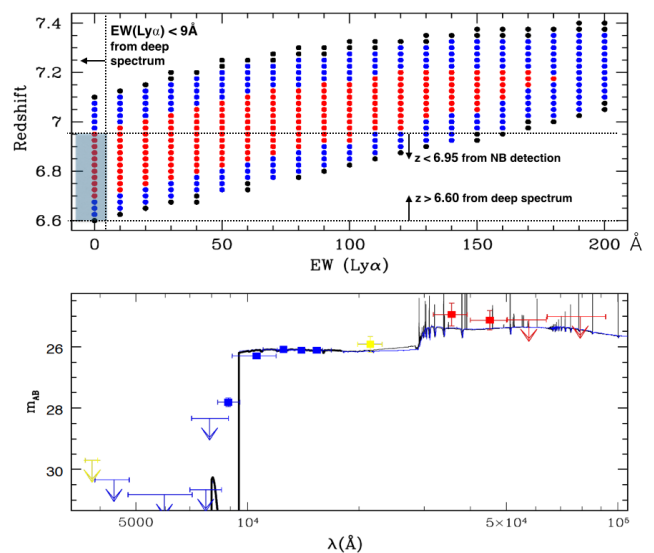


Fig. 2. Top: The projected Redshift- $EW(Ly\alpha)$ solutions of the SED fitting are shown. Black, blue and red symbols represent 3-, 2-, and 1-sigma solutions. The well detected signal in the z_{850} -band is reproducible with large $EW(Ly\alpha)$ at higher redshift ($z > 7$) or very faint $Ly\alpha$ emission at the lower redshift, $z < 7$. Upper and lower horizontal dotted lines mark the limits provided by the NB973 detection and non-continuum detection below $z = 6.6$ in the deep spectrum, respectively. The vertical dotted line marks the upper limit of the $Ly\alpha$ rest-frame equivalent width. The transparent gray region underlines the most probable redshift interval. **Bottom:** SED fitting performed with BC03 libraries with (thin black) and without (blue) nebular emission lines are shown. The fit to the HST bands only is shown with the thick black line. Blue, yellow and red points represent photometry from HST, VLT (U and K bands) and Sptizer/IRAC, respectively. Upper limits at one sigma are marked with arrows.

tinuum, $z_{MAX} = (9755 - 100)/1215.7 - 1 = 6.94$ (see inset of Figure 3).

3.1. A deep upper limit to the $Ly\alpha$ flux

Given the above upper limit z_{MAX} , the FORS2+600z configuration provides a safe constraint on the $Ly\alpha$ line flux.¹ Indeed, there are no obvious spectral features in the three S/N spectra at the position of the *G2_1408* (marked by arrows), neither in the combined one (see Figure 1).

We note that these deeper data do not confirm the tentative detection of a weak line located at $\lambda = 9691.5 \pm 0.5\text{\AA}$, corresponding to a redshift of 6.972 that we reported in Fontana et al. (2010) with $S/N < 7$ (and shown with a circle in the F18 spectrum of Figure 1). Exploiting the RMS map we derived, the reliability of the spectral feature in the F18 spectrum turns out to have $S/N \simeq 4.5$. In the combined (52h) spectrum, however, the S/N at the same wavelength position is even smaller, $\lesssim 3$, and suggests that the earlier tentative detection was most probably a noise spike.

To assign a statistical significance to our 52h non-detection, we estimated the minimum line flux reachable with the deep FORS2+600z spectrum by computing simulations as in V11 and P14. Two dimensional asymmetric $Ly\alpha$ lines have been inserted

¹ As an example Figure 1 shows the secondary object in B7 spectrum in which the $H\alpha$ line is detected at $z=0.535$ consistently with the $z_{phot} = 0.5$, and showing that the FORS2+600z configuration is still performing well at $\sim 10100\text{\AA}$.

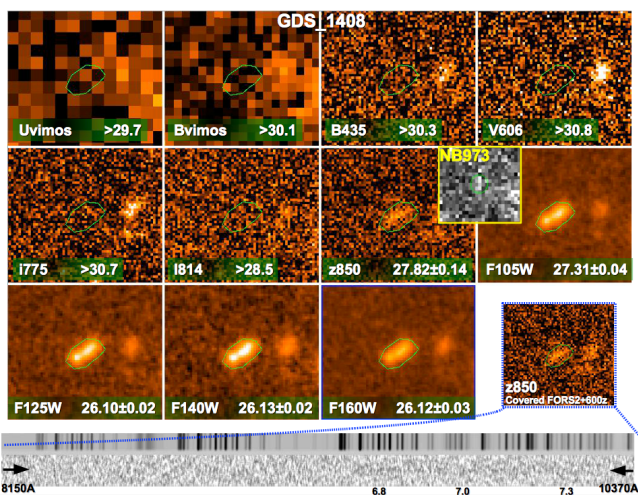


Fig. 3. The cutouts ($3'' \times 3''$) from U to H-band of *G2_1408* are shown with the magnitudes (limits are at one-sigma). The green contour marks the galaxy's shape as a guidance. The inset image placed between the z_{850} and F105W refer to the narrow band filter NB973 in which the source is detected (3-sigma). The bottom-right cutout shows the clear detection in the z_{850} band ($S/N \sim 8$), for which there is a good coverage of the ultra-deep FORS2 spectrum (also reported in the bottom).

in the science raw frames moving the line from $z = 5.7$ to 7.3 with $dz = 0.0013$ (i.e., one pixel at the given spectral resolution), including the dithering pattern, varying the FWHM and the line flux, convolving with spectral resolution along the dispersion and with the seeing along the spatial direction (extracted from the header of each science frame). Knowing the exact position of the inserted lines in the raw frames (that by definition include also the cosmic rays), and including the full reduction pipeline process and the response curve, we can reliably access the limits attainable by the instrument. The resulting S/N of the simulated lines are fully compatible with those we observed at redshift 6 and 7 (P11, P14 and V11).

The upper limit we derive from the combined $52h$ spectrum is $f(Ly\alpha) < 3 \times 10^{-18} \text{ erg/s/cm}^2$ at 3-sigma (in the sky-lines) and up to 9-sigma (in sky-free regions) in the whole wavelength range, i.e., up to $z = 7.0$ (see Figure 4). Adopting the $F125W=26.10\pm0.02$ as the estimation of the continuum under the $Ly\alpha$ line, and given the relatively flat UV slope in the near infrared bands, the limit on the $Ly\alpha$ flux corresponds to an upper limit on the equivalent width $EW < 9 \text{ \AA}$, with the same statistical accuracy. It represents the faintest limit on the $Ly\alpha$ flux ever derived at $z > 6.5$.

While absorption lines are clearly impossible to detect in our spectra, it is worth to investigate whether the non detection of the continuum in the $52h$ spectrum is compatible with the expected magnitude ≈ 26.1 . To this aim, a set of two-dimensional continua (with flat UV slope) without any absorption line have been added to the raw frames as performed for line simulations, adopting a Gaussian profile in the spatial direction (consistent with the observed seeing). They have been added to the raw frames with dithering and dimmed in magnitude, from 23.0 to 27.0 with $dm = 0.25$ (in all the process the response curve has been taken into account). Figure 4 shows the results. The S/N decreases accordingly with the magnitude dimming and in the presence of sky emission lines, becoming impossible to detect at magnitude ≈ 26.0 unless the object is at redshift below 6.6 (see Figure 4). Both simulations on $Ly\alpha$ line and continuum show the clear decrease of the S/N at the position of sky emission lines,

i.e., it is lower where the sky emission is stronger. The results of the continuum simulation are in line with the observed faint galaxies, in particular with those we confirmed in P11 at $z \sim 6$ based on continuum-break only.

3.2. Refined redshift

Depending on its EW, the $Ly\alpha$ emission can contribute significantly to the broad band photometry and as a consequence to the photometric redshift determination. In particular, the flux observed in the z_{850} band (see Figure 3) depends on the position of the $Ly\alpha$ -line/break (i.e., the redshift), the IGM attenuation, the EW of the possible $Ly\alpha$ emission ($EW(Ly\alpha)$), and mildly on the UV slope of the source, β ($F_\lambda = \lambda^\beta$). With the depth and photometric quality available for this galaxy and the upper limit derived above, the redshift value can be refined. To this aim we performed the SED fitting with Bruzual & Charlot (2003)(BC03, hereafter) templates by including different equivalent widths of the $Ly\alpha$ (0-200Å rest-frame) and focusing solely on the break between the optical and near infrared bands, i.e., B_{435} , V_{606} , i_{775} , z_{850} , F_{105W} , F_{125W} , F_{140W} and F_{160W} . We have not included the NB filter in this exercise since its photometry is not as accurate as the HST data. The templates adopted a range of e -folding star-formation timescales ranging from 0.1 to 15 Gyr (the latter being in practice a constant-star formation history), metallicities from $Z = 0.2Z_\odot$ to $Z = Z_\odot$, and a Calzetti attenuation curve with $A_V = 0 - 3$. Figure 2 shows the *plane* (redshift- $EW(Ly\alpha)$), in which the degeneracy is clear, i.e., a progressively stronger $Ly\alpha$ emission is required at increasing redshifts to compensate for the increasing absorption by the IGM. The degeneracy with the $Ly\alpha$ line is broken by including the result from the ultra-deep $52h$ spectrum discussed in Sect. 3.1, that forces the $EW(Ly\alpha)$ to be smaller than 9 \AA rest-frame. Once the $Ly\alpha$ constraints are included, the redshift of *G2_1408* is constrained within 6.7 and 6.95 at 1σ and 6.6 and 7.1 at 2σ . The top panel of Figure 2 shows the resulting region where the redshift would lie, that is $z = 6.82^{+0.1}_{-0.1}$ (at one sigma).

We note that the 2σ range is consistent with the continuum-only simulations described above and the non detection in the sky-free region of the spectrum at $9000\text{\AA} < \lambda < 9280\text{\AA}$, that both suggest a lower limit of the redshift, $z_{MIN} = 6.6$. Less significant, but consistent with z_{MIN} , is the slightly brighter $3.6\mu\text{m}$ magnitude to respect the $4.5\mu\text{m}$ channel in the data we have, that could suggest a flux boost of the $[\text{OIII}]4959-5007+H\beta$ structure in the first channel, while the $H\alpha$ line is outside (redward) the second one, respectively. Indeed, this is confirmed with deeper IRAC data, in which a clear break has been measured, $[3.6 - 4.5]\mu\text{m} = 0.66 \pm 0.2$ (Smit et al. in preparation, Labbé et al. (2013)). This is fully consistent with our redshift estimation.

The SED fitting with and without the nebular component has then been performed including the IRAC and ground based photometry. We have included the full treatment of the nebular emission (both in lines and continuum), computed using the Schaerer & de Barros (2009) model, as described in Castellano et al. (2014). The resulting SED fits with HST-only bands and the whole photometry are shown in the bottom panel of Figure 2. The derived physical quantities in the various cases agree within a factor of two. This exercise provides an estimate of the stellar mass of $M = 5^{+3}_{-2} \times 10^9 M_\odot$, an age $\approx 0.1^{+0.15}_{-0.05}$ Gyr, a dust attenuation $E(B-V) \approx 0.1 \pm 0.05$ and a dust corrected star formation rate of $21^{+20}_{-10} M_\odot \text{ yr}^{-1}$.

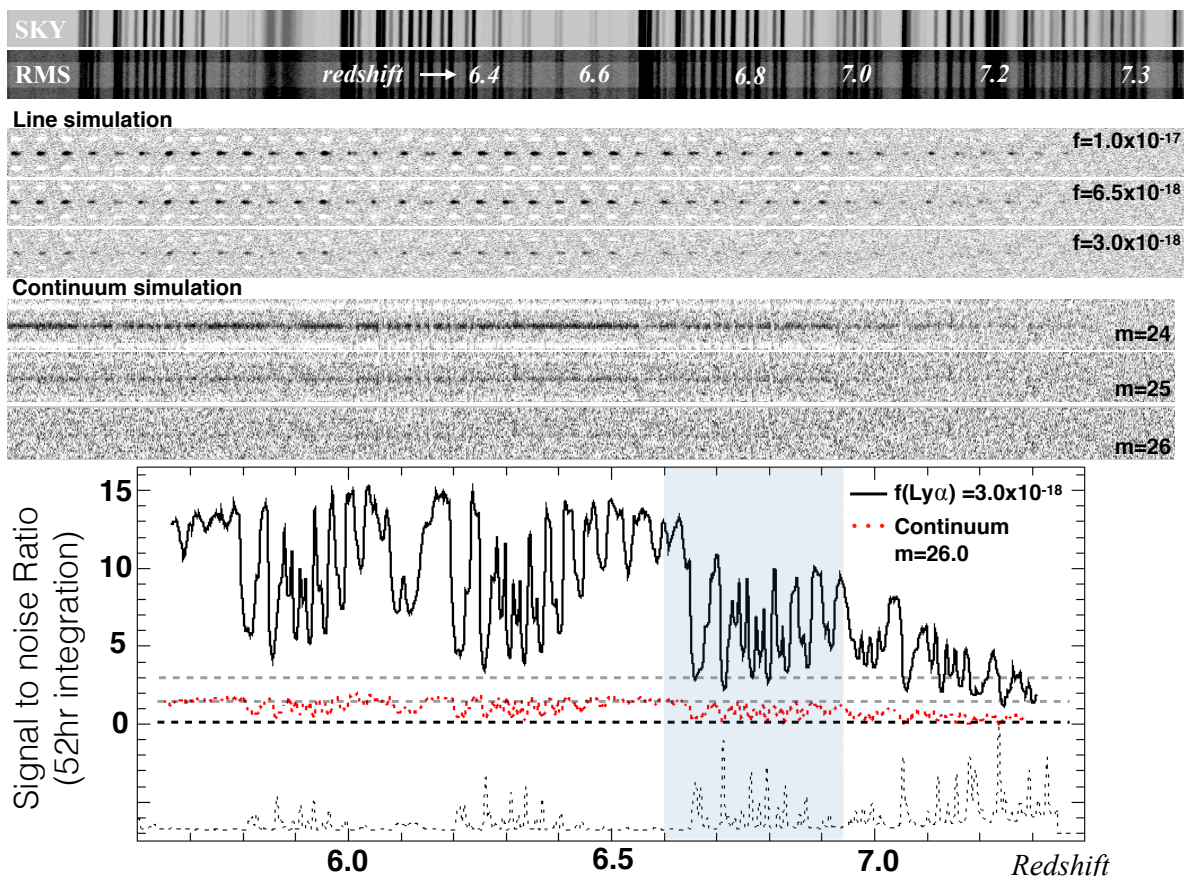


Fig. 4. Simulation of the expected signal to noise ratio for emission $Ly\alpha$ line and continuum with 52 hours integration with FORS2. From top to bottom: the two dimensional spectra of the sky and RMS map are shown as an example and guidance for the eye. Simulated signal to noise 2d-spectra of line emission (snapshot) and continuum emissions are shown, with indicated the line flux and magnitude at the (flat) continuum on the right. It is clear that the S/N is lower where the sky lines are stronger. In the bottom part the S/N ratio of the $Ly\alpha$ feature versus redshift (solid black line) and the continuum (red dotted line) are reported for the case of *GDS_1408*. The transparent grey region marks the $z_{MIN} < z < z_{MAX}$ interval, see text for more details. Grey horizontal dotted lines mark $S/N = 1.5$ and 3.0 .

4. Discussion

The combination of excellent photometry and ultradeep spectroscopic data lead us to conclude that the lack or extreme weakness of a $Ly\alpha$ emission is a real feature of this object. It is therefore worth investigating the reasons why the $Ly\alpha$ line is not present.

4.1. The effective $Ly\alpha$ escape fraction

Dijkstra & Jeason-Daniel (2013) differentiate between the term ‘escape’ fraction and ‘effective escape’ fraction of $Ly\alpha$ photons, $f_{esc}(Ly\alpha)$ and $f_{esc}^{eff}(Ly\alpha)$, respectively. The former being related to the transport of photons out of the galaxy’s interstellar medium, while the latter includes further damping by the IGM, giving rise to a low-surface-brightness $Ly\alpha$ glow around galaxies. Therefore, $f_{esc}^{eff}(Ly\alpha)$ can be much smaller than $f_{esc}(Ly\alpha)$. If we assume “normal” metallicities and IMFs, and that on average star formation is ongoing at equilibrium ($age > 100 Myrs$ with constant SFR), an estimation of the $Ly\alpha$ luminosity can be obtained imposing $SFR(UV)/SFR(Ly\alpha) \approx 1$ (Hayes et al. 2011; Verhamme et al. 2008). Assuming the SFR(UV) corrected by dust extinction is representative of the total ongoing star formation activity, the intrinsic $Ly\alpha$ flux turns out to be $\approx 4 \times 10^{-17} \text{ ergs}^{-1} \text{ cm}^{-2}$, i.e., $EW(Ly\alpha)$ rest-frame $\approx 120 \text{ \AA}$. The upper limit on the observed $Ly\alpha$ line flux derived above corresponds to an observed $EW(Ly\alpha) < 9 \text{ \AA}$ rest-frame (at $3 - 9\sigma$), 13

times smaller than the expected intrinsic emission, that gives an upper limit of $f_{esc}^{eff}(Ly\alpha) < 8\%$.

4.2. What is attenuating the $Ly\alpha$ emission ?

The escape of $Ly\alpha$ photons from a gaseous and dusty interstellar medium is a complex process which depends sensitively on a number of physical properties, such as dust and gas mass, star formation rate, metallicity, kinematic, escaping ionizing radiation, as well as the gas geometry and filling factor and the galaxy orientation (Neufeld 1991; Verhamme et al. 2008; Verhamme et al. 2012; Hayes et al. 2011; Yajima et al. 2014; Laursen et al. 2013; Dijkstra et al. 2014). Additionally, the neutral hydrogen in the IGM can scatter part of the $Ly\alpha$ photons and decrease the line luminosity. For example, Laursen et al. (2011) suggested that the average IGM transmission could be $\approx 20\%$ at $z = 6.5$. Also in this case the transmission depends sensitively on the viewing angle and the environments of the galaxy, as it is affected by the inhomogeneous filamentary structure of IGM. At $z > 6.5$ the IGM damping could be the dominant effect.

It is not possible to investigate in detail the above quantities with the current information. Therefore we have to rely on global properties, e.g., by performing a comparative analysis with lower redshift galaxies at $z > 3 - 4$. First, it has been shown that $2 < z < 6$ UV-bright star-forming galaxies ($L > L^*$) show on

average a deficit of $Ly\alpha$ emission with respect the fainter UV counterparts (e.g., Ando et al. 2006; Vanzella et al. 2009; Lee et al. 2013; Balestra et al. 2010), explained by the fact that on average galaxies that are intrinsically brighter in the UV are also more star forming and more massive, more chemically enriched and thus more likely to be obscured by dust, especially the $Ly\alpha$ resonant transition that is expected to be efficiently absorbed. A decreasing trend of $f_{esc}(Ly\alpha)$ emission with increasing E(B-V) has also been observed in several studies (Giavalisco et al. 1996; Atek et al. 2008; Verhamme et al. 2008; Kornei et al. 2010; Hayes et al. 2011). The observed UV slope ($\beta = -2$) of *GDS_1408* suggests there is a dust attenuation $A_{1600} \sim 1.3$ (Castellano et al. 2014; de Barros et al. 2014). The inferred $SFR \approx 21 M_{\odot} yr^{-1}$ and assuming the Schmidt law (Schmidt 1959; Kennicutt 1998a), implies a non negligible amount of gas, $M_{gas} \approx 3 \times 10^9 M_{\odot}$, comparable to the stellar mass, and would favor a more efficient $Ly\alpha$ photon destruction operated by dust. The presence of dust and gas would also suggest that the escape fraction of ionizing radiation is very low, as it has been observed in L^* star-forming galaxies at $z \approx 3$ (Vanzella et al. 2010a; Boutasia et al. 2011).

Second, *GDS_1408* is one of the more extended sources among the $z \sim 7$ candidates (half light radius of $0.26''$, i.e., 1.4 proper Kpc, Grazian et al. 2011, with an elongated morphology of 4.8×2.5 proper Kpc, see Figure 3). It has been shown that the $Ly\alpha$ equivalent width and the size observed at the 1500\AA rest-frame of the stellar continuum anti-correlate, such that on average the emitters appear more compact and nucleated than the non-emitters, with average half light radius $\lesssim 1\text{ kpc}$ (Law et al. 2007; Vanzella et al. 2009; Pentericci et al. 2010).

GDS_1408 is moderately star-forming and contains a non negligible amount of dust, it is UV bright and spatially extended. While we cannot exclude that the CGM/IGM plays an additional role, the properties of *GDS_1408* are consistent with those of others lower- z L^* star-forming galaxies that show faint $Ly\alpha$ emission, and is not a “smoking gun” of an increased neutral IGM at $z = 7$. It is worth noting that we are discussing a single galaxy case which clearly cannot be considered as representative of a population. The deficit of $Ly\alpha$ lines from redshift 6 to 7 recently observed is significant and is based on a statistical analysis that compares tens of star-forming galaxies selected with very similar color techniques, independently from the presence of the $Ly\alpha$ line. However, as noted also in Schenker et al. (2014), galaxies like *GDS_1408* are not the best tracers of an IGM damping. The higher is the probability the $Ly\alpha$ emission is internally absorbed, the lower is the power of tracing the neutral gas fraction of the circum/inter-galactic medium.

Nonetheless, it is important to assess the nature of “continuum-only” star-forming galaxies at $z > 6.5$, still an unexplored line of research. As reported in this work, the tentative spectroscopic investigation of “continuum-only” galaxies at $z > 6.5$ shows all the limitations of the 8-10 meter class telescopes coupled with optical spectroscopy ($\lambda < 1.1\mu\text{m}$). Different and future facilities are needed to shed light on their nature.

4.3. Future prospects: ALMA, JWST and ELT

We have shown the current limits of 8-10m class telescopes in the spectroscopic characterization and redshift measurement of non- $Ly\alpha$ emitters at $6.6 < z < 7.3$. If $z \sim 7$ is a critical value above which the visibility of $Ly\alpha$ lines decreases drastically, then future facilities are necessary to capture the UV continuum-break and the ultraviolet absorption lines and/or optical nebular

emission lines at $7 < z < 10$. JWST-NIRSPEC will probe the typical nebular emission lines, e.g., [OII]3727, $H\beta$, [OIII]4959-5007 up to $z \approx 9$ ($5\mu\text{m}$) and the extremely large telescopes (ELT, 30-40m diameter) will allow us to cover the mid-infrared part (e.g., EELT-METIS, 8-14 μm) and to probe the UV continuum with $S/N=10$ down to $J \approx 27$ and therefore to study in detail the ultraviolet absorption lines, not to mention the possibility to perform high spatial resolution analysis.

In particular, the case of *GDS_1408* is shown in Figure 5, where a schematic view of the limits on the continuum at $S/N=10$ are reported for the ELT, JWST and VLT telescopes. A good characterization of the ultraviolet absorption lines will be feasible with the ELT. JWST would marginally identify the trace of the continuum ($S/N < 5$), but will open for the measure of optical emission lines (up to [OIII]4959-5007).

While JWST and ELT will definitely perform these kind of studies, at present the measure of the redshift with 8-10m telescopes could be achieved looking at emission lines different from $Ly\alpha$. Though unusual, lines like [OIII] $\lambda\lambda$ 1661-1666 and [CIII] $\lambda\lambda$ 1907-1909 could be identified by means of near infrared spectrographs. Moreover, depending on the source of ionizing photons, other lines like NV 1240, [NIV] $\lambda\lambda$ 1483-1486, CIV 1550, HeII 1640 can also be measured (e.g., Osterbrock & Ferland 2006; Vanzella et al. 2010b; Raiter et al. 2010; Steidel et al. 2014).

Another promising facility that might be able to determine the spectroscopic redshift of this galaxy is ALMA. Indeed, a spectral scan of the [CII]158 μm line encompassing the full 2-sigma range of uncertainty could be covered with two ALMA spectral bands. Assuming that the local SFR -[CII]158 μm relation of Sargsyan et al. (2012) holds also at these high redshifts, based on the best-fitting $SFR=20M_{\odot}/yr^{-1}$ we expect a flux of 0.24 Jy km/s, that can be secured in a relatively short time (< 6 hours in the Cycle2 sensitivity) with ALMA. A molecular line scan that covers the 3mm window (89-115 GHz) can also reveal multiple CO transitions in *GDS_1408*. In particular at $z > 6.5$ the transitions $J = 7 \rightarrow 6$ and $J = 6 \rightarrow 5$ (where J is the rotational quantum number) are observable. Given the UV slope and the star formation activity, and assuming the relation between CO line luminosity and SFR (see Carilli & Walter 2013; Decarli et al. 2014), the expected CO transitions can be detected ($S/N \gtrsim 3$) with an ALMA 3mm scan with sensitivity limit of 0.1 mJy beam^{-1} .

5. Conclusions

We have reported the combined VLT/FORS2 spectroscopy of one of the most reliable $z \approx 7$ galaxy candidates in the Hubble Ultra Deep Field. Three different programs at VLT targeted *GDS_1408* in the last five years, for a total integration time of 52h. We have retrieved from the ESO archive all these data, and re-analyzed them in a consistent way. Our main results are:

1. **An upper limit on the $Ly\alpha$ emission:** We are able to place a stringent upper limit of $f(Ly\alpha) < 3 \times 10^{-18} \text{ erg/s/cm}^2$ at 3-sigma (in the sky-lines) and up to 9-sigma (in sky-free regions) in the whole wavelength range, i.e., up to $z = 7.0$ (see Figure 4). This corresponds to an upper limit on the equivalent width $EW < 9 \text{\AA}$, with the same statistical accuracy. With the deeper data used here we do not confirm the tentative detection of a weak line located at $\lambda = 9691.5 \pm 0.5 \text{\AA}$, corresponding to a redshift of 6.972, that we claimed in F10.
2. **Redshift refinement:** The combination of ultra-deep spectroscopy, superb HST information and narrow band imag-

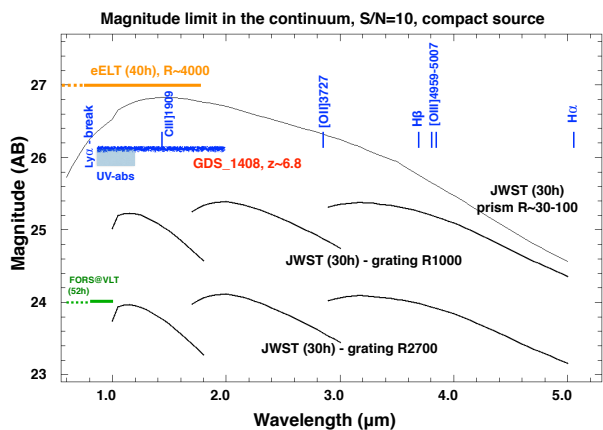


Fig. 5. Expected magnitude limits in the continuum ($S/N=10$) with 30-50h integration time are shown for ELT, (orange, Evans et al. 2013), JWST (black, available in tabular form <http://www.stsci.edu/jwst/instruments/nirspec/sensitivity/>) and VLT-FORS (green, this work). The estimated limit for KMOS is magnitude ≈ 21.5 in the YJ band with 50h integration (rescaling from the KMOS manual, Sect. 2.3.4). The schematic position of *GDS_1408* is reported (blue), with the continuum magnitude ≈ 26.1 , the typical ultraviolet absorption lines from the $Ly\alpha$ to CIV 1550 (grey region, UV-abs) and the basic emission lines, e.g., [OIII]1909, [OIII]3727, $H\beta$, [OIII]4959-5007 and $H\alpha$.

ing, have allowed us to refine the photometric redshift value of *GDS_1408*, that turns out to be 6.82 ± 0.1 . The same analysis indicate that *GDS_1408* has a nearly solar metallicity and is relatively dust attenuated ($A_{1600} \approx 1$) galaxy.

- $Ly\alpha$ escape fraction:** We derived a $f_{esc}^{eff}(Ly\alpha) < 8\%$. The $Ly\alpha$ attenuation can be a combination of internal (ISM) and external effects (IGM).

Even though we cannot rule out a major contribution of the IGM in damping the line, the *most* plausible interpretation is that *G2_1408* is a star-forming galaxy at $z \approx 6.82$ moderately evolved and containing sufficient gas and dust to attenuate the $Ly\alpha$ emission, before it reaches the intergalactic medium. If compared with fainter ($0.05L^* < L < 0.2L^*$), young, less massive and less evolved counterparts that show $Ly\alpha$ emission and much steeper UV slopes $\beta < -2.5$ (e.g., Balestra et al. 2013; Vanzella et al. 2014), *G2_1408* appears more massive and evolved ($\beta \approx -2$).

An absence of the line due to dust absorption is not in contrast with recent results on the deficit of $Ly\alpha$ lines ascribed to a possible increase of the neutral gas fraction of the IGM between $z \sim 6$ and 7 (e.g., P11, P14, Finkelstein et al. 2013). In fact, the apparent drop of lines is an evidence based on statistical samples, in which the properties of redshift 6 and 7 galaxies are compared in a differential way, and applying similar color selection techniques.

Redshift 7 sources like *GDS_1408*, and in general even fainter ones at $J = 27$, will be well studied spectroscopically with ELT and JWST telescopes, in particular for what concerns the UV absorption lines and nebular (optical) emission lines, respectively. As an example, JWST will provide the systemic redshift from rest-frame optical nebular emission lines (Oxygen, Balmer lines) and the ELT will capture the signature of the ISM in absorption in the rest-frame ultraviolet. This will be feasible not before 2018-2020. Currently, a facility that can provide redshift measures at $z \gtrsim 7$ and characterize the properties of the ISM

and stellar population is ALMA. Sources like *GDS_1408* with a reliable guess on the redshift value are suitable candidates for the scanning mode of ALMA.

Acknowledgements. We thanks R. Bouwens for providing information about the deep IRAC magnitudes of the source and P. Oesch for providing information about the *GDS_1408* target in the spectroscopic program 088.A-1008(A). We thank F. Vito, M. Mignoli, A. Cimatti and S. de Barros for useful discussions. Part of this work has been funded through the INAF grants (PRIN INAF 2012).

References

- Ando, M., Ohta, K., Iwata, I., et al. 2006, *ApJ*, 645, L9
- Atek, H., Kunth, D., Hayes, M., Östlin, G., Mas-Hesse, J. M., 2008, *A&A*, 488, 491A
- Atek, H., Kunth, D., Schaerer, D., Mas-Hesse, J. M., Hayes, M., Östlin, G., Kneib, J.-P., *A&A*, accepted
- Balestra, I., Mainieri, V., Popesso, P., et al. 2010, *A&A*, 512, A12
- Balestra, I., Vanzella, E., Rosati, P., et al. 2013, *A&A*, 559, L9
- Behrens, C., Dijkstra, M., & Niemeyer, J. C. 2014, *A&A*, 563, A77
- Bolton, J. S., & Haehnelt, M. G. 2013, *MNRAS*, 429, 1695
- Boutsia, K., Grazian, A., Giallongo, E., et al. 2011, *ApJ*, 736, 41
- Bouwens, R. J., Illingworth, G. D., Blakeslee, J. P., Broadhurst, T. J., & Franx, M. 2004, *ApJ*, 611, L1
- Bouwens, R. J., & Illingworth, G. D. 2006, *Nature*, 443, 189
- Bouwens, R. J., Illingworth, G. D., Franx, M., & Ford, H. 2008, *ApJ*, 686, 230
- Bouwens, R. J., Illingworth, G. D., Oesch, P. A., Labbé, I., Trenti, M., van Dokkum, P., Franx, M., Stiavelli, M., Carollo, C. M., Magee, D., Gonzalez, V., 2011, *ApJ*, 737, 90B
- Bouwens, R. J., Illingworth, G. D., Oesch, P. A., et al. 2014, *arXiv:1403.4295*
- Bruzual, G., & Charlot, S. 2003, *MNRAS*, 344, 1000
- Bunker, A., Wilkins, S., Ellis, R., et al. 2010, *MNRAS*, 409, 855
- Carilli, C. L., & Walter, F. 2013, *ARA&A*, 51, 105
- Caruana, J., Bunker, A. J., Wilkins, S. M., Stanway, E. R., Lorenzoni, S., Jarvis, M. J., Elbert, H., *MNRAS* in press, 2013, (arXiv/1311.0057C)
- Calzetti, D., Armus, L., Bohlin, R. C., et al. 2000, *ApJ*, 533, 682
- Castellano, M., Fontana, A., Boutsia, K., et al. 2010a, *A&A*, 511, 20
- Castellano, M., Fontana, A., Grazian, A., et al. 2012, *A&A*, 540, A39
- Castellano, M., Sommariva, V., Fontana, A., et al., 2014, *A&A*, in press, (arXiv-1403.0743)
- de Barros, S., Schaerer, D., & Stark, D. P. 2014, *A&A*, 563, A81
- Decarli, R., Walter, F., Carilli, C., et al. 2014, *ApJ*, 782, 78
- Dijkstra, M., & Wyithe, J. S. B. 2010, *MNRAS*, 408, 352
- Dijkstra, M., Mesinger, A., Wyithe, J. S. B., 2011, *MNRAS*, 414, 2139
- Dijkstra, M., & Jeesson-Daniel, A. 2013, *MNRAS*, 435, 3333
- Dijkstra, M., Wyithe, S., Haiman, Z., Mesinger, A., & Pentericci, L. 2014, *MNRAS*, 440, 3309
- Duval, F., Schaerer, D., Östlin, G., Laursen, P., 2013, *A&A*, accepted
- Evans, C., Puech, M., Barbu, B., Bastian, N., Bonifacio, P., Caffau, E., Cuby, Jean-Gabriel, Dalton, G., Dunlop, J., Flores, H., Hammer, F., Kaper, L. et al., 2013, White paper presented at the “Shaping E-ELT Science & Instrumentation”
- Fontana, A., Vanzella, E., Pentericci, L., et al. 2010, *ApJ*, 725, L205
- Finkelstein, S. L., Papovich, C., Giallisco, M., et al. 2010, *ApJ*, 719, 1250
- Finkelstein, S. L., Papovich, C., Dickinson, M., et al. 2013, *Nature*, 502, 524
- Giallisco, M., Koratkar, A., Calzetti, D., 1996, *ApJ*, 466, 831G
- Grazian, A., Castellano, M., Koekemoer, A. M., Fontana, A., Pentericci, L., Testa, V., Boutsia, K., Giallisco, M., Santini, P., 2011, *A&A*, 532, 33G
- Hayes, M., Schaerer, D., Östlin, G., Mas-Hesse, J. M., Atek, H., Kunth, D., 2011, *ApJ*, 730, 8H
- Kornei, K. A., Shapley, A. E., Erb, D. K., Steidel, C. C., Reddy, N. A., Pettini, M., Bogosavljević, M., 2010, *ApJ*, 711, 693K
- Kennicutt, R. C., Jr. 1998, *ApJ*, 498, 541
- Kennicutt, R. C., Jr. 1998, *ARA&A*, 36, 189
- Inoue, A. K. 2011, *MNRAS*, 415, 2920
- Labbé, I., Bouwens, R., Illingworth, G. D., & Franx, M. 2006, *ApJ*, 649, L67
- Labbé I., Oesch P. A., Bouwens R. J., Illingworth G. D., Magee D., González V., Carollo C. M., Franx M., Trenti M., van Dokkum P. G., Stiavelli, M., 2013, *ApJ*, 777, 19
- Laursen, P., Sommer-Larsen, J., & Razoumov, A. O. 2011, *ApJ*, 728, 52
- Laursen, P., Duval, F., & Oumlstlin, G. 2013, *ApJ*, 766, 124
- Law, D. R., Steidel, C. C., Erb, D. K., et al. 2007, *ApJ*, 656, 1
- Lee, K.-S., Dey, A., Cooper, M. C., Reddy, N., & Jannuzi, B. T. 2013, *ApJ*, 771, 25
- Loeb, A., Barkana, R., & Hernquist, L. 2005, *ApJ*, 620, 553
- McLure, R. J., Dunlop, J. S., Cirasuolo, M., et al. 2010, *MNRAS*, 403, 960

- McLure, R. J., Dunlop, J. S., Bowler, R. A. A., Curtis-Lake, E., Schenker, M., Ellis, R. S., Robertson, B. E., Koekemoer, A. M., Rogers, A. B., et al., 2013, *MNRAS*, 432, 2696
- Miralda-Escudé, J., Haehnelt, M., Rees, M. J., 2000, *ApJ*, 530, 1
- Nakajima, K., & Ouchi, M. 2013, arXiv:1309.0207, *MNRAS*, in press
- Neufeld, D. A. 1991, *ApJ*, 370, L85
- Oesch, P. A., Bouwens, R. J., Illingworth, G. D., et al. 2010, *ApJ*, 709, L16
- Ono, Y., Ouchi, M., Mobasher, B., Dickinson, M., Penner, K., Shimasaku, K., Weiner, B. J., Kartaltepe, J. S., Nakajima, K., Nayyeri, H., et al., 2012, *ApJ*, 744, 830
- Osterbrock, D. E. 1989, *Astrophysics of Gaseous Nebulae and Active Galactic Nuclei* (Univ. Science Books, Mill Valley, CA, USA)
- Osterbrock D.E. & Ferland, G. J., 2006, *Astrophysics of gaseous nebulae and active galactic nuclei*, 2nd. ed. by D.E. Osterbrock and G.J. Ferland. Sausalito, CA: University Science Books, 2006
- Ouchi, M., Shimasaku, K., Akiyama, M., Simpson, C., Saito, T., Ueda, Y., Furusawa, H., et al., 2008, *ApJS*, 176, 301
- Pentericci, L., Grazian, A., Scarlata, C., et al. 2010, *A&A*, 514, A64
- Pentericci, L., Fontana, A., Vanzella, E., Castellano, M., Grazian, A., Dijkstra, M., Boutsia, K., Cristiani, S., Dickinson, M., Giallongo, E., et al. 2011, *ApJ*, 743, 132
- Pentericci, L., Vanzella, E., Fontana, A., et al. 2014, arXiv:1403.5466
- Raiter, A., Schaerer, D., & Fosbury, R. A. E. 2010, *A&A*, 523, A64
- Rauch, M., Becker, G. D., Haehnelt, M. G., Gauthier, J.-R., Ravindranath, S., Sargent, Wallace L. W., 2011, *MNRAS*, 418, 1115R
- Robertson, B. E., Ellis, R. S., Dunlop, J. S., McLure, R. J., Stark, D. P., 2010, *Nature*, 468, 49
- Sargsyan, L., Leboutteiller, V., Weedman, D., Spoon, H., et al., 2012, *ApJ*, 755, 171
- Schaerer, D. 2003, *A&A*, 397, 527
- Schaerer, D. & de Barros, S., 2009, *A&A*, 502, 423
- Schaerer D., de Barros S., Stark D. P., 2011, *A&A*, 536, A72
- Schenker, M. A., Stark, D. P., Ellis, R. S., Robertson, B. E., Dunlop, J. S., McLure, R.J., Kneib, J.-P., Richard, J., 2012, *ApJ*, 744, 179S
- Schenker, M. A., Ellis, R. S., Konidaris, N. P., & Stark, D. P. 2014, arXiv:1404.4632
- Schmidt, M. 1959, *ApJ*, 129, 243
- Shibuya, T., Kashikawa, N., Ota, K., Iye, M., Ouchi, M., Furusawa, H., Shimasaku, K., Hattori, T., 2012, *ApJ*, 752, 114
- Siana, B., Teplitz, H. I., Colbert, J., et al. 2007, *ApJ*, 668, 62
- Stark, D. P., Ellis, R. S., & Ouchi, M. 2011, *ApJ*, 728, L2
- C. C. Steidel, G. C. Rudie, A. L. Strom, M. Pettini, N. A. Reddy, A. E. Shapley, R. F. Trainor, D. K. Erb, M. L. Turner, N. P. Konidaris, K. R. Kulas, G. Mace, K. Matthews, I. S. McLean, 2014, *ApJin press*, (arxiv/1405.5473)
- Taylor & Lidz, 2013, in press
- Treu, T., Trenti, M., Stiavelli, M., Auger, M. W., Bradley, L. D., 2012, *ApJ*, 747, 27
- Treu, T., Schmidt, K. B., Trenti, M., Bradley, L. D., Stiavelli, M., 2013, *ApJ*, 775, 29
- Vanzella, E., Giavalisco, M., Dickinson, M., Cristiani, S., Nonino, M., Kuntschner, H., Popesso, P., Rosati, P., Renzini, A., et al., 2009, *ApJ*, 695, 1163
- Vanzella, E., Giavalisco, M., Inoue, A. K., et al. 2010, *ApJ*, 725, 1011
- Vanzella E., Grazian A., Hayes M., Pentericci L., Schaerer D., Dickinson M., Cristiani S., Giavalisco M., Verhamme A., Nonino M., Rosati P., 2010, *A&A*, 513, 20
- Vanzella, E., Pentericci, L., Fontana, A., Grazian, A., Castellano, M., Boutsia, K., Cristiani, S., Dickinson, M., et al., 2011, *ApJ*, 730, 35
- Vanzella, E., Guo, Y., Giavalisco, M., Grazian, A., Castellano, M., Cristiani, S., Dickinson, M.; Fontana, A., Nonino, M., Giallongo, E., et al., 2012, *ApJ*, 751, 70
- Vanzella, E., Fontana, A., Zitrin, A., et al. 2014, *ApJ*, 783, L12
- Verhamme, A., Schaerer, D., Atek, H., Tapken, C., 2008, *A&A*, 491, 89V
- Verhamme, A., Dubois, Y., Blaizot, J., et al. 2012, *A&A*, 546, A111
- Verhamme, A., Orlitova, I., Schaerer, D., & Hayes, M. 2014, arXiv:1404.2958
- Yan, H., & Windhorst, R. A. 2004, *ApJ*, 612, L93
- Yan, H., Windhorst, R., Hathi, N., et al. 2010, *RAA*, 10, 867
- Yajima, H., Li, Y., Zhu, Q., et al. 2014, *MNRAS*, 440, 776
- Wilkins, S. M., Bunker, A. J., Lorenzoni, S., et al. 2011, *MNRAS*, 411, 23
- Zackrisson, E., Inoue, A. K., & Jensen, H. 2013, *ApJ*, 777, 39